LIMNOLOGY AND OCEANOGRAPHY
Letters

ASLO
Open Access

Limnology and Oceanography Letters 2024

doi: 10.1002/lol2.10388

LETTER

Concentration and compositional controls on degradation of permafrost-derived dissolved organic matter on the Qinghai–Tibetan Plateau

Yinghui Wang [1,2,3]* *Yasong Wang*,[1] *Lulu Han*,[1] *Amy M. McKenna* [3,4] *Anne M. Kellerman* [3] *Robert G. M. Spencer* [3] *Yuanhe Yang* [5] *Yunping Xu* [1]*

[1]College of Marine Sciences, Shanghai Ocean University, Shanghai, China; [2]State Environmental Protection Key Laboratory of Integrated Surface Water-Groundwater Pollution Control, School of Environmental Science and Engineering, Southern University of Science and Technology, Shenzhen, China; [3]National High Magnetic Field Laboratory Geochemistry Group and Department of Earth, Ocean, and Atmospheric Science, Florida State University, Tallahassee, Florida, USA; [4]Department of Soil and Crop Sciences, Colorado State University, Fort Collins, Colorado, USA; [5]State Key Laboratory of Vegetation and Environmental Change, Institute of Botany, Chinese Academy of Sciences, Beijing, China

Scientific Significance Statement

Dissolved organic matter (DOM) derived from permafrost is a substantial carbon source in aquatic ecosystems worldwide, yet its reactivity remains incompletely understood. This study advances our understanding of permafrost DOM, focusing on samples from the Qinghai–Tibetan Plateau and examining its behavior during biodegradation and photodegradation. We reveal unique lability patterns within DOM components and underscore the pivotal role of dissolved organic carbon concentration in shaping its fate. These insights are not only crucial for managing greenhouse gas release from permafrost regions but also hold broader significance for understanding carbon dynamics in aquatic systems globally, contributing to improved carbon cycling models and environmental management strategies.

Abstract

Understanding the fate of permafrost-derived dissolved organic matter (DOM) is critical for unraveling its role in carbon cycling. However, it remains unclear whether the high lability of permafrost-derived DOM can be attributed to intrinsic chemical properties or elevated carbon concentrations. We investigated the dynamics of permafrost DOM from the Qinghai–Tibetan Plateau using both biodegradation and photodegradation experiments. Biodegradation and photodegradation of permafrost-derived DOM exhibited distinct qualitative

*Correspondence: wangyh@sustech.edu.cn; ypxu@shou.edu.cn

Associate editor: Janne Karlsson

Author Contribution Statement: YPX contributed to the conceptualization of the research and acquiring funding for this work. YHW, YSW, and LLH contributed to experimental performance. AMM, AMK, and RGMS contributed to the FT-ICR MS analysis and FT data interpretation. YHW, YSW, YPX, YHY, and RGMS contributed to interpreting the results and writing/editing the manuscript.

Data Availability Statement: All 21 T negative-ion electrospray ionization mass spectra files and elemental composition assignments are publicly available via the Open Science Framework at https://osf.io/264cz/.

Additional Supporting Information may be found in the online version of this article.

preferences for specific chemical groups (i.e., peptide-like and aromatics, respectively). Notably, reducing the initial concentration of dissolved organic carbon (DOC) by half and a quarter resulted in shifts in biodegradable DOC content from 11.2% to 11.5% and 8.5%, respectively, accompanied by a corresponding decrease in the biodegradation rate from 0.11 to 0.06 and 0.03. This insight highlights the importance of recognizing the interplay between DOM quality and concentration and bears broader significance for our understanding of the fate of permafrost-derived DOM in natural ecosystems.

Permafrost soils store a significant amount of organic carbon (OC), equivalent to almost double the amount of carbon in the atmosphere (Tarnocai et al. 2009; Schuur et al. 2015; Mishra et al. 2021). The alpine permafrost on the Qinghai–Tibet Plateau (QTP) represents the second largest permafrost carbon reservoir after the Arctic, containing approximately 15–33 Pg C in the top 3 m depth (Mu et al. 2015; Ding et al. 2016; Wang et al. 2020*a*). However, rapid warming has led to permafrost thaw and degradation of the QTP (Mu et al. 2017; Liu et al. 2022). Permafrost OC can be degraded in situ or removed through aquatic biogeochemical processes such as photodegradation, biodegradation, and organic matter flocculation (Feng et al. 2013; Qu et al. 2017), thereby significantly increasing the emissions of greenhouse gases such as CO_2 and CH_4 (Yang et al. 2018; Estop-Aragonés et al. 2020; Wang et al. 2022). While the biolability and photolability of permafrost OC upon thawing are well-established (Vonk et al. 2013; Mann et al. 2015; Spencer et al. 2015; Ward and Cory 2016), investigations using terrestrial biomarkers and radiocarbon dating have revealed the persistence of a portion of permafrost OC during transport to large rivers and oceans (Feng et al. 2013; Qu et al. 2017).

Persistence of dissolved organic matter (DOM) in the environment relies on both intrinsic molecular properties and extrinsic environmental factors (Bercovici et al. 2021; Dittmar et al. 2021; Berggren et al. 2022), but the relative importance of each factor remains elusive (Arrieta et al. 2015; Jiao et al. 2015; Shen and Benner 2020). Recent advances in analytical techniques, including Fourier-transform ion cyclotron resonance mass spectrometry (FT-ICR MS), have revealed a correlation between the high degradability of permafrost DOM and specific molecular characteristics (Mann et al. 2015; Ward and Cory 2016). However, the concentration of organic matter exerts a notable influence on microbial decomposition. The trade of gaining and losing energy directs microbes toward a preference for chemically labile and easily accessible components (Jannasch 1994). In soil, increasing the concentration of organic matter by approximately 2.5 times stimulates microbial respiration, resulting in a 66% increase (Hernandez and Hobbie 2010). In the deep sea, the extremely low concentration of organic matter poses a limitation for microbial utilization of potentially active organic compounds (Jannasch 1994; Arrieta et al. 2015). Notably, permafrost thaw streams have been shown to exhibit extremely high dissolved organic carbon (DOC) concentrations, orders of magnitude higher than that regularly reported in marine and inland aquatic ecosystems, with values often greater than 100 mg C L^{-1} (Vonk et al. 2013; Mann et al. 2015; Spencer et al. 2015; Wang et al. 2018*a*). However, beyond the known compositional effects, the extent to which these elevated DOC concentrations contribute to the rapid loss of permafrost OC remains uncertain, adding complexity to the understanding of permafrost carbon fate in large rivers and oceans.

In this study, we conducted bioincubation and photodegradation experiments using DOM extracted from alpine permafrost on the northeast QTP. In addition, we employed a concentration gradient approach to dilute the DOC concentration for bioincubations. By applying multiple methods, we aim to elucidate the differences in chemical transformations of alpine permafrost DOM between the biodegradation and photodegradation processes and assess biodegradation efficiency in relation to carbon concentration. Our study seeks to advance the comprehension of permafrost DOM fate, thereby expanding the scope to encompass the unique characteristics associated with alpine permafrost DOM on the northeast QTP.

Methods

Experimental settings

We extracted permafrost DOM from 2 kg of permafrost soil using 10 L of ultrapure water (18 MΩ cm) at 4°C for 24 h. The permafrost soil was collected from a deep exposed soil profile with a depth exceeding 1 m on the QTP (37°28′38.84″, 100°17′30.70″). The extracts underwent sequential filtration through pre-combusted GF/A (1.6 μm) and GF/F (0.7 μm) membranes (Whatman), followed by 0.22 μm polyethersulfone membrane filtration (Millipore). The 1.6 μm filtrate was used as an inoculum for the biodegradation experiments. All filtrates were stored at 4°C until set up for incubation within a week. For additional sampling and incubation details, refer to Supporting Information Text S1.

We conducted laboratory biodegradation incubations following methods adapted from Mann et al. (2012) and Wickland et al. (2012). The inoculum solution was mixed with 0.22 μm filtrate in a 1:100 volume ratio. Portions of the mixed solutions were diluted to 50% and 25% of the original DOC concentration by adding ultrapure water. These non-diluted and diluted systems, which represent 100%, 50%, and 25% of the original DOC concentration, showed consistent inoculum size per unit DOC and were denoted as 100%-DOC, 50%-DOC, and 25%-DOC groups, respectively. Subsequently, 100 mL of each solution was transferred into pre-cleaned and pre-combusted 300 mL glass bottles. Incubation bottles were

tightly secured to limit evaporation but were opened weekly to ensure adequate oxygen supply during incubation at 20°C. After specific time intervals (0, 7, 14, 21, and 28 d), we harvested three identical bottles from each group. Collected samples were filtered through pre-combusted 0.7 μm GF/F membranes and stored frozen (−20°C) and in the dark for subsequent analyses.

For the photodegradation experiments, we filled pre-combusted quartz flasks with 500 mL of 0.22 μm filtrate and sealed them with parafilm. Photochemical irradiations were conducted using natural sunlight (Ward et al. 2017). All flasks were placed on the laboratory roof (Shanghai, China) in September and irradiated for 15 d. Samples were collected at different time intervals (0, 3, 6, 9, and 15 d), corresponding to sunlight exposure times of approximately 0, 22, 38, 61, and 106 h. After filtration through a 0.22 μm filter, the filtrates were stored frozen (−20°C) and in the dark.

Sample analysis

DOC concentration was analyzed on a Shimadzu TOC-VCPH analyzer. Optical properties were assessed using a Shimadzu dual-beam UV-2600 spectrophotometer and a Hitachi F-7000 fluorimeter. The detailed analytical methods have been described (Wang et al. 2018*b*). Fluorescence excitation–emission matrices were processed using the parallel factor analysis (PARAFAC) method (Murphy et al. 2013). Optical characteristics were determined by calculating specific UV–visible absorbance at 254 nm ($SUVA_{254}$), spectral slope ($S_{275–295}$), fluorescence index (FI), biological index (BIX), and humification index (HIX) (McKnight et al. 2001; Ohno 2002; Weishaar et al. 2003; Helms et al. 2008; Wilson and Xenopoulos 2009).

The molecular level composition of DOM was determined by 21 T FT-ICR MS at the National High Magnetic Field Laboratory (Tallahassee, FL, USA) (Hendrickson et al. 2015; Smith et al. 2018). Analytical methods are described in Supporting Information Text S2 (Xian et al. 2010; Blakney et al. 2011; Savory et al. 2011; Spencer et al. 2014). Elemental compositions were assigned using PetroOrg© software (Corilo 2015) based on the presence of carbon, hydrogen, oxygen, nitrogen, and sulfur, with mass accuracies of less than 0.4 ppm. The modified aromaticity index (AI_{mod}) was calculated to assess aromaticity (Koch and Dittmar 2016). Formulae were classified into five different chemical groups: condensed aromatics, polyphenolics, highly unsaturated compounds, aliphatics, and peptide-like compounds based on elemental composition (Kellerman et al. 2015). The formulae with $AI_{mod} \geq 0.5$ were denoted as aromatic formulae, which were a combination of condensed aromatics and polyphenolics. The relative abundance of each compound class was weighted by intensities. Formulae with $H/C \geq 1.5$ (molecular lability boundary) were denoted as labile molecules and were used to calculate the lability index (MLB_L) based on the relative intensity (D'Andrilli et al. 2010).

Results and discussion

Changes in DOM with biodegradation

In the undiluted system (A), the initial DOC concentration was 23.18 ± 0.20 mg L^{-1} (mean ± standard deviation). Over 7 d, it decreased to 22.52 ± 0.25 mg L^{-1} and further decreased significantly to 20.48 ± 0.08 mg L^{-1} over 14 d ($p = 0.01$). The slower initial DOC consumption could be attributed to the "bottle effect", a common phenomenon when the microbial community is perturbed upon being introduced to the bottle environment (Allison and Martiny 2008). Alternatively, a control group without inoculum could offer insights into background changes, aiding in the resolution of degradation kinetics. In the absence of a control experiment, we collectively considered background changes and biodegradation, fitting the biodegradation process with a one-phase exponential decay function (refer to Supporting Information Text S3). Biodegradable DOC accounted for 11.2% of total DOC in QTP permafrost (Fig. 1a), a proportion notably lower than that reported for Arctic permafrost (34–47%) (Vonk et al. 2013; Mann et al. 2015; Spencer et al. 2015). The diminished biodegradability observed in QTP permafrost may be attributed to the relatively high abundance of refractory humic DOM, which would limit the degradation in permafrost DOM incubations (Shirokova et al. 2019). In addition, the lower biodegradability in our study may stem from a more advanced degradation state of permafrost organic matter in the QTP, as evidenced by higher alkyl-C abundance and higher alkyl/O-alkyl ratio than Arctic soil (Wang et al. 2020*b*).

Three components C1 (maxima em/ex: 424 nm/240 nm), C2 (476 nm/260 nm), and C3 (334 nm/275 nm) were validated with PARAFAC analysis and assigned as reprocessed microbially related humic-like substances, terrestrially derived humic-like substances, and protein-like substances, respectively (Stedmon et al. 2003; Guo et al. 2011). The relative abundance of C1 (67.3–67.8%) and C2 (24.6–24.8%) increased slightly ($p < 0.05$), while that of C3 decreased from 8.2% to 7.5% ($p < 0.01$, Fig. 2), suggesting preferential biodegradation of the biolabile protein-like component. In addition, the $S_{275–295}$ gradually increased from 15.02×10^{-3} to 15.46×10^{-3} nm^{-1} ($p < 0.01$), indicating conversion from high molecular weight DOM to low molecular weight DOM (Mann et al. 2015). However, the relative abundance of colored DOM (a_{350}) and fluorescent DOM (Fmax) remained largely unchanged throughout the incubation period, and $SUVA_{254}$, FI, BIX, and HIX values did not display a clear variation trend (Fig. 1d–f). This suggests that the biodegradation's impact on the quantity of colored DOM components might be minimal, and optical characteristics may not reveal significant changes during that biodegradation.

Along with decreased C3 and increased $S_{275–295}$, the changes observed in the DOM remained consistent at the molecular level. The relative abundance of peptide-like compounds slightly decreased from 1.7% to 1.4%, and the intensity-weighted average molecular weight of DOM changed from 398 to 386 Da. The biodegradation also led to the

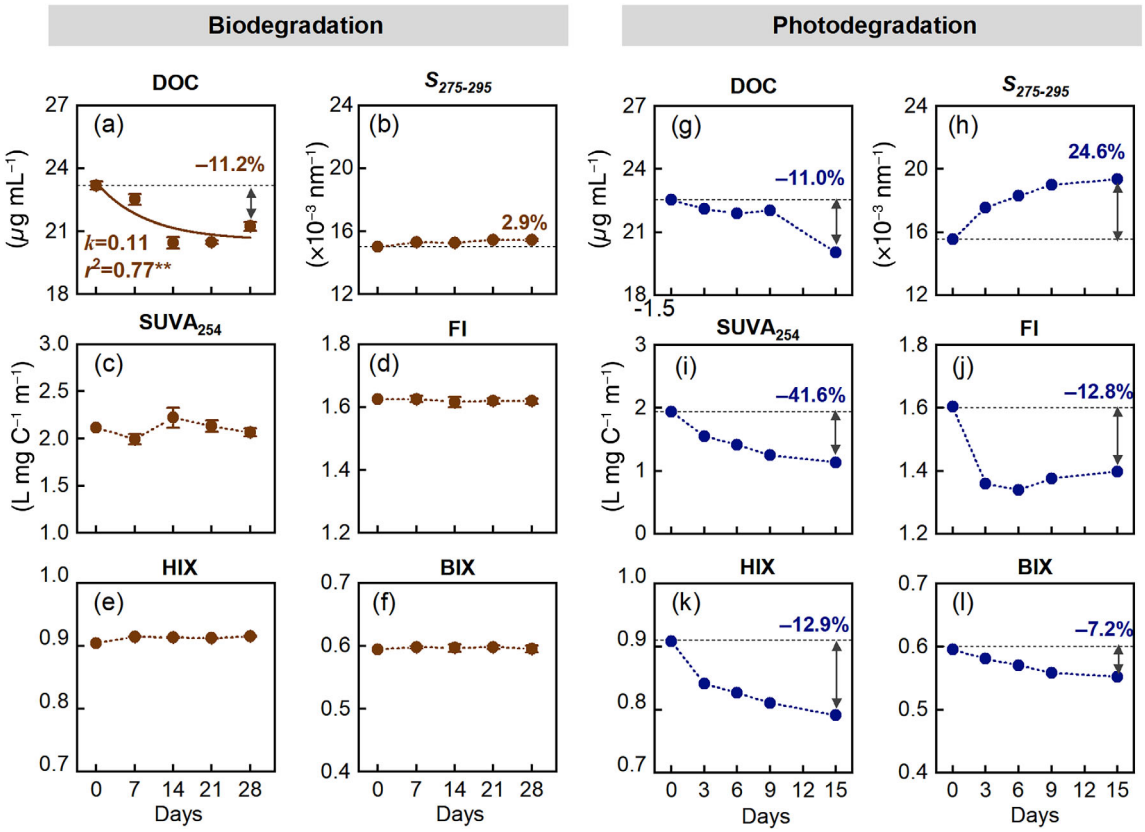

Fig. 1. The changes in the concentration and optical characterization of dissolved organic carbon (DOC) over time during biodegradation (**a–f**) and photodegradation (**g–l**) experiments. The horizontal dotted lines represent the values in the initial samples, and the numbers displayed on the figures indicate significant changes relative to the parameters in the initial samples. One-phase exponential decay function is used to fit the biodegradation processes, and the degradation rate was expressed as the *k* value (d^{-1}).

loss of 1967 formulae, including 576 labile formulae (H/C > 1.5) and 587 aromatic formulae (AI_{mod} > 0.5), constituting 24.5% of the labile formulae (n = 2349) and 11.6% of the aromatic formulae (n = 5042) present in the initial samples, respectively. Furthermore, the relative abundances of condensed aromatic increased from 8.2% to 10.1% (Fig. 3). Integrating perspectives from optical characteristics and molecular signatures, our results support the preferential consumption and transformation of high molecular weight protein-like DOM while preserving aromatic compounds during biodegradation (Spencer et al. 2014; Grunert et al. 2021).

Changes in permafrost leachate DOM with photodegradation

Over 15 d, photodegradation reduced the DOC concentration from 22.53 mg L^{-1} to 20.05 mg L^{-1} (Fig. 1g). However, the DOC concentration did not reach a plateau, suggesting incomplete photodegradation, so we did not perform decay function fitting. For the first 9 d, the DOC changes were relatively slow, which might result from partial photodegradation that alters only DOM composition, not concentration (Cory et al. 2014), and also might be due to relatively low available quantum yields in natural irradiation as the cloud cover, aerosol loading, and water vapor changed during the incubation (Yang et al. 2021; Yu et al. 2023).

Due to the photodegradation, the $S_{275–295}$ increased significantly by 22.3%, while the $SUVA_{254}$, FI, HIX, and BIX all decreased by 41.6%, 12.8%, 12.9%, and 7.2%, respectively (Fig. 1i–l). Terrestrial humic-like C2 decreased by 31.2%, while the protein-like C3 demonstrated a twofold increase from 7.9% to 17.5% (Fig. 2). These results indicate selective preservation or slower decay of protein-like DOM and preferential removal of humic-like DOM during photodegradation.

At the molecular level, consistent with decreases in $SUVA_{254}$ and the relative abundance of humic-like C2, the relative abundance of condensed aromatics and polyphenolics revealed by FT-ICR MS also decreased from 5.5% to 3.7% and 13.9% to 10.5%, respectively, during photodegradation. This is further supported by a decrease in AI_{mod} (0.30–0.26). However, the relative abundance of peptide-like formulae increased from 1.4% to 2.9%, and MLB_L increased from 9.3% to 13.4%. Moreover, 1279 formulae were lost after photodegradation (Fig. 3d), including 630 aromatic formulae and 89 labile formulae, accounting for 18.3% of the aromatic formulae and 4.5% of

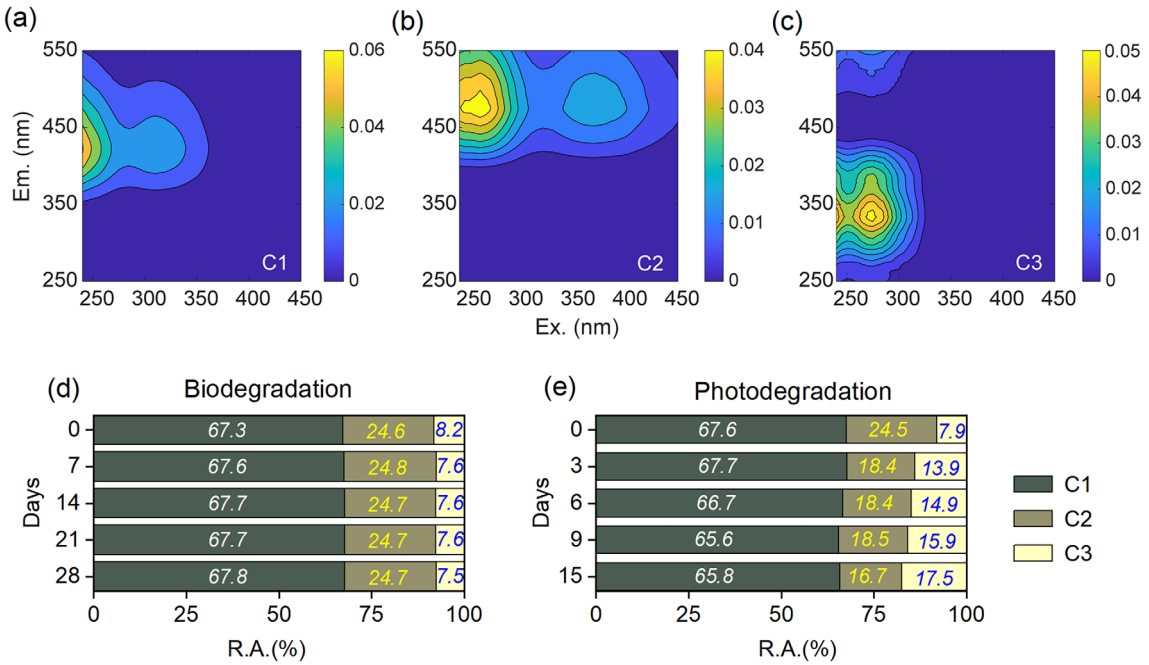

Fig. 2. Contour plots of three identified EEM-PARAFAC components (**a**–**c**), each characterized by different excitation and emission wavelengths. The relative abundances (R.A.) of these components during the biodegradation and photodegradation processes are shown in the stacked bar chart (**d**, **e**). Specifically, component C1 represents reprocessed microbial-related humic-like substances, component C2 corresponds to terrestrially derived humic-like substances, and component C3 signifies protein-like substances.

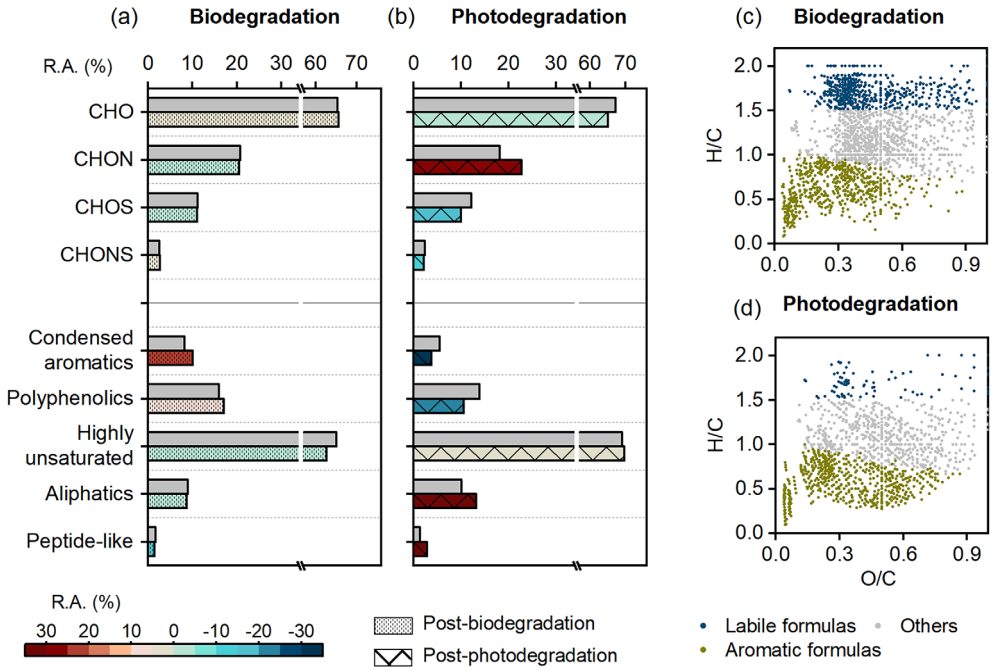

Fig. 3. The changes in the relative abundance (R.A.) of compositional groups before and after the biodegradation (**a**) and photodegradation (**b**) experiments. Van Krevelen plots are provided for the formulas that were lost after biodegradation (**c**) and photodegradation (**d**), with labile formulas and aromatic formulas highlighted in different colors.

the labile formulae present in initial samples. Compared to biodegradation (11.6% and 24.5% loss of aromatic and labile formulae), preferential photodegradation of aromatic formulae was evident, while aliphatic and peptide-like formulae had higher bioreactivity but were less prone to photodegradation (Cory and Kling 2018; Grunert et al. 2021). Furthermore, the co-occurrence of photo- and biodegradation might synergistically contribute to DOC loss, involving partial photo-oxidation of high molecular weight aromatic DOM to less condensed forms, potentially increasing biolability (Cory and Kling 2018).

Effect of permafrost DOM concentration on biodegradation

The biodegradation of 100%-DOC–25%-DOC groups exhibited exponential decay ($r^2 > 0.75$; Fig. 4a–c). Biodegradable DOC was similar across 100%-DOC and 50%-DOC

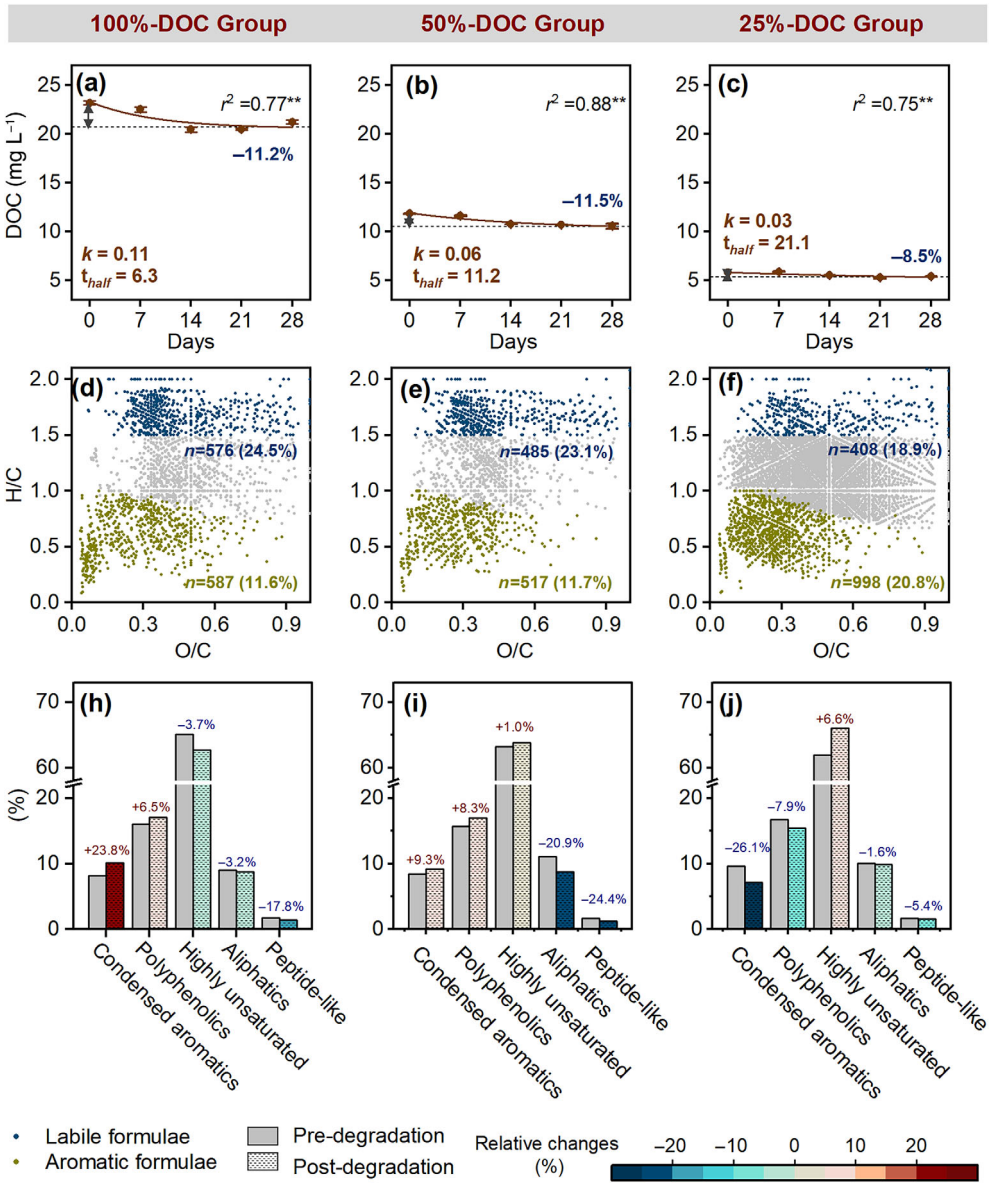

Fig. 4. The changes in dissolved organic carbon (DOC) concentration during biodegradation in different groups with varying high-to-low DOC concentrations (100%-DOC, 50%-DOC, and 25%-DOC). A one-phase exponential decay function is used to fit the biodegradation processes, and the degradation rate and half-time were expressed as the *k* value and t_{half}. The error bars showed standard deviations of DOC concentration from three repeats. Van Krevelen plots are presented for the formulas that were lost at the end of the experiment for different groups, with labile formulas highlighted in red and carboxyl-rich alicyclic molecules highlighted in blue (**d–f**). The "*n*" values indicate the number of molecules and the relative changes compared to initial samples. The relative abundance of different chemical groups in pre- and post-degraded samples for different groups (**h–j**). The color gradient indicates the relative changes compared to the initial samples.

groups (11.2% and 11.5%), but it decreased to 8.5% in the 25%-DOC group. In addition, the degradation rates were influenced by the initial DOC concentration. As the initial DOC concentrations decreased from 100%-DOC to 25%-DOC, the half-life (t_{half}) increased from 6.3 to 11.2 d and then to 21.1 d, and the degradation rate (k value) decreased from 0.11 to 0.06 d^{-1} and then to 0.03 d^{-1} (Fig. 4a–c). The concentration of microbes in 100%-DOC–25%-DOC groups exhibited a synchronous decrease with the DOC concentration due to dilution. The dilution method employed in this study may have introduced limitations in terms of microbial concentration and the availability of inorganic micro- and macronutrients for the microbial community. However, in soil systems, the solid (soil)/solution (ultrapure water) ratio of 0.1 is commonly utilized in extractions for subsequent biodegradation incubations (Kalbitz et al. 2003; Bowen et al. 2009), and our 100%-DOC–25%-DOC groups demonstrated solid/solution ratios ranging from 0.2 to 0.05, which deviate from the conventional ratio and may not impose strict restrictions on microbial concentrations and inorganic nutrient availability during incubation. While the potential effect of microbial concentration on decreasing degradation rates cannot be entirely ruled out, our findings suggest that the lower DOC concentration could be an effective impactor as it showed restrictions on microbial growth efficiency (Eiler et al. 2003; Arrieta et al. 2015).

From a molecular formulae perspective, different changes occurred in different DOC concentration groups after 28 d of biodegradation. 100%-DOC, 50%-DOC, and 25%-DOC groups experienced a loss of 1967, 1645, and 2183 formulae, respectively (Fig. 4d–f). Among those completely degraded formulae, 587, 517, and 998 were identified as aromatic formulae, accounting for 11.6%, 11.7%, and 20.8% of the total aromatic formulae in the related initial samples of different groups. Also, we recognized 576, 485, and 408 labile formulae in these completely degraded formulae, which represent 24.5%, 23.08%, and 18.9% of the total labile formulae in the related initial samples of different groups. Consistently, the AI_{mod} and the relative abundance of all aromatic formulae in 100%-DOC and 50%-DOC groups increased, while they all decreased in 25%-DOC group with the biodegradation (Fig. 4h–j). The relative abundance of peptide-like formulae in undegraded samples of 100%-DOC to 25%-DOC groups were 1.7%, 1.6%, and 1.6%, and with biodegradation, it decreased by 17.8%, 24.4%, and 5.4%. Compared with the 100%-DOC and 50%-DOC groups, the 25%-DOC group exhibited higher consumption of aromatic formulae during low-carbon concentration biodegradation.

The differences in degradation rates and chemical compositions observed during biodegradation processes among the three groups highlight the crucial role of DOC concentration and DOC composition. In the 100%-DOC and 50%-DOC groups, where the absolute content of DOC substrates is comparatively high, microorganisms exhibit an active preference for energetically favorable substrates, thereby opting to utilize unstable peptide-like substances present in the environment. Conversely, in the 25%-DOC group, where the absolute concentration of DOM substrates is lower, microbial survival mechanisms, driven by energy considerations, lead to a tendency for passive uptake of randomly encountered substrates to maintain metabolism rather than actively seeking and consuming energetically favorable substrates (Jannasch 1994; Arrieta et al. 2015). Given the higher relative concentration of aromatic compounds compared to peptide-like substances under these conditions, the consumption of aromatic compounds significantly increases compared to the other two groups. Our findings support the notion that the carbon concentration impacts the lability of DOM (Eiler et al. 2003; Arrieta et al. 2015; Lennartz and Dittmar 2022). These findings provide important insights into the role of DOC concentration on the biodegradability of DOM and the mechanisms underlying the transformation of different types of DOM formulae.

Conclusion

Our study uncovers distinct biolability and photolability patterns within specific components of permafrost DOM from the QTP. In addition, it confirms that the relatively low concentration of DOC restricts the accessibility of permafrost organic matter, influencing microbial biodegradation pathways, which is possibly associated with microbial energy utilization strategies. The observed DOC concentration-dependent shifts indicate that both concentration and compositional characteristics significantly impact carbon turnover rates, particularly during the long-distance transport of permafrost-derived DOC from source regions to the sea with continuous dilution. Understanding the intricate connections between DOC concentration, microbial activity, and DOM transformation is pivotal for the accurate modeling of carbon fluxes in diverse ecosystems, further underscoring the relevance of our findings in the context of global biogeochemical cycles.

References

Allison, S. D., and J. B. H. Martiny. 2008. Resistance, resilience, and redundancy in microbial communities. Proc. Natl. Acad. Sci. USA **105**: 11512–11519. doi:10.1073/pnas.0801925105

Arrieta, J. M., E. Mayol, R. L. Hansman, G. J. Herndl, T. Dittmar, and C. M. Duarte. 2015. Dilution limits dissolved organic carbon utilization in the deep ocean. Science **348**: 331–333. doi:10.1126/science.1258955

Bercovici, S. K., M. C. Arroyo, D. De Corte, T. Yokokawa, and D. A. Hansell. 2021. Limited utilization of extracted dissolved organic matter by prokaryotic communities from the subtropical North Atlantic. Limnol. Oceanogr. **66**: 2509–2520. doi:10.1002/lno.11769

Berggren, M., and others. 2022. Unified understanding of intrinsic and extrinsic controls of dissolved organic carbon reactivity in aquatic ecosystems. Ecology **103**: e3763. doi:10.1002/ecy.3763

Blakney, G. T., C. L. Hendrickson, and A. G. Marshall. 2011. Predator data station: A fast data acquisition system for advanced FT-ICR MS experiments. Int. J. Mass Spectrom. **306**: 246–252. doi:10.1016/j.ijms.2011.03.009

Bowen, S. R., E. G. Gregorich, and D. W. Hopkins. 2009. Biochemical properties and biodegradation of dissolved organic matter from soils. Biol. Fertil. Soils **45**: 733–742. doi:10.1007/s00374-009-0387-6

Corilo, Y. 2015. *EnviroOrg*. Florida State Univ.

Cory, R. M., C. P. Ward, B. C. Crump, and G. W. Kling. 2014. Sunlight controls water column processing of carbon in arctic fresh waters. Science **345**: 925–928. doi:10.1126/science.1253119

Cory, R. M., and G. W. Kling. 2018. Interactions between sunlight and microorganisms influence dissolved organic matter degradation along the aquatic continuum. Limnol. Oceanogr.: Lett. **3**: 102–116. doi:10.1002/lol2.10060

D'Andrilli, J., T. Dittmar, B. P. Koch, J. M. Purcell, A. G. Marshall, and W. T. Cooper. 2010. Comprehensive characterization of marine dissolved organic matter by Fourier transform ion cyclotron resonance mass spectrometry with electrospray and atmospheric pressure photoionization. Rapid Commun. Mass Spectrom. **24**: 643–650. doi:10.1002/rcm.4421

Ding, J., and others. 2016. The permafrost carbon inventory on the Tibetan Plateau: A new evaluation using deep sediment cores. Glob. Change Biol. **22**: 2688–2701. doi:10.1111/gcb.13257

Dittmar, T., S. T. Lennartz, H. Buck-Wiese, D. A. Hansell, C. Santinelli, C. Vanni, B. Blasius, and J.-H. Hehemann. 2021. Enigmatic persistence of dissolved organic matter in the ocean. Nat. Rev. Earth Environ. **2**: 570–583. doi:10.1038/s43017-021-00183-7

Eiler, A., S. Langenheder, S. Bertilsson, and L. J. Tranvik. 2003. Heterotrophic bacterial growth efficiency and community structure at different natural organic carbon concentrations. Appl. Environ. Microbiol. **69**: 3701–3709. doi:10.1128/Aem.69.7.3701-3709.2003

Estop-Aragonés, C., and others. 2020. Assessing the potential for mobilization of old soil carbon after permafrost thaw: A synthesis of ^{14}C measurements from the northern permafrost region. Glob. Biogeochem. Cycles **34**: e2020GB006672. doi:10.1029/2020gb006672

Feng, X., and others. 2013. Differential mobilization of terrestrial carbon pools in Eurasian Arctic river basins. Proc. Natl. Acad. Sci. USA **110**: 14168–14173. doi:10.1073/pnas.1307031110

Grunert, B. K., M. Tzortziou, P. Neale, A. Menendez, and P. Hernes. 2021. DOM degradation by light and microbes along the Yukon River-coastal ocean continuum. Sci. Rep. **11**: 10236. doi:10.1038/s41598-021-89327-9

Guo, W., L. Yang, H. Hong, C. A. Stedmon, F. Wang, J. Xu, and Y. Xie. 2011. Assessing the dynamics of chromophoric dissolved organic matter in a subtropical estuary using parallel factor analysis. Mar. Chem. **124**: 125–133. doi:10.1016/j.marchem.2011.01.003

Helms, J. R., A. Stubbins, J. D. Ritchie, E. C. Minor, D. J. Kieber, and K. Mopper. 2008. Absorption spectral slopes and slope ratios as indicators of molecular weight, source, and photobleaching of chromophoric dissolved organic matter. Limnol. Oceanogr. **53**: 955–969. doi:10.4319/lo.2008.53.3.0955

Hendrickson, C. L., and others. 2015. 21 Tesla Fourier transform ion cyclotron resonance mass spectrometer: A national resource for ultrahigh resolution mass analysis. J. Am. Soc. Mass Spectrom. **26**: 1626–1632. doi:10.1007/s13361-015-1182-2

Hernandez, D. L., and S. E. Hobbie. 2010. The effects of substrate composition, quantity, and diversity on microbial activity. Plant Soil **335**: 397–411. doi:10.1007/s11104-010-0428-9

Jannasch, H. W. 1994. The microbial turnover of carbon in the deep-sea environment. Glob. Planet. Change **9**: 289–295. doi:10.1016/0921-8181(94)90022-1

Jiao, N., and others. 2015. Comment on "Dilution limits dissolved organic carbon utilization in the deep ocean". Science **350**: 1483. doi:10.1126/science.aab2713

Kalbitz, K., J. Schmerwitz, D. Schwesig, and E. Matzner. 2003. Biodegradation of soil-derived dissolved organic matter as related to its properties. Geoderma **113**: 273–291. doi:10.1016/S0016-7061(02)00365-8

Kellerman, A. M., D. N. Kothawala, T. Dittmar, and L. J. Tranvik. 2015. Persistence of dissolved organic matter in lakes related to its molecular characteristics. Nat. Geosci. **8**: 454–457. doi:10.1038/Ngeo2440

Koch, B. P., and T. Dittmar. 2016. From mass to structure: An aromaticity index for high-resolution mass data of natural organic matter. Rapid Commun. Mass Spectrom. **30**: 250. doi:10.1002/rcm.7433

Lennartz, S. T., and T. Dittmar. 2022. Controls on turnover of marine dissolved organic matter-testing the null hypothesis of purely concentration-driven uptake: Comment on Shen and Benner, "Molecular properties are a primary control on the microbial utilization of dissolved organic matter in the ocean". Limnol. Oceanogr. **67**: 673–679. doi:10.1002/lno.12028

Liu, F., S. Qin, K. Fang, L. Chen, Y. Peng, P. Smith, and Y. Yang. 2022. Divergent changes in particulate and mineral-associated organic carbon upon permafrost thaw. Nat. Commun. **13**: 5073. doi:10.1038/s41467-022-32681-7

Mann, P. J., A. Davydova, N. Zimov, R. G. M. Spencer, S. Davydov, E. Bulygina, S. Zimov, and R. M. Holmes. 2012. Controls on the composition and lability of dissolved organic matter in Siberia's Kolyma River basin. J. Geophys. Res.: Biogeosci. **117**. doi:10.1029/2011jg001798

Mann, P. J., T. I. Eglinton, C. P. McIntyre, N. Zimov, A. Davydova, J. E. Vonk, R. M. Holmes, and R. G. M. Spencer.

2015. Utilization of ancient permafrost carbon in headwaters of Arctic fluvial networks. Nat. Commun. **6**: 7856. doi:10.1038/ncomms8856

McKnight, D. M., E. W. Boyer, P. K. Westerhoff, P. T. Doran, T. Kulbe, and D. T. Andersen. 2001. Spectrofluorometric characterization of dissolved organic matter for indication of precursor organic material and aromaticity. Limnol. Oceanogr. **46**: 38–48. doi:10.4319/lo.2001.46.1.0038

Mishra, U., and others. 2021. Spatial heterogeneity and environmental predictors of permafrost region soil organic carbon stocks. Sci. Adv. **7**: eaaz5236. doi:10.1126/sciadv.aaz5236

Mu, C., T. Zhang, Q. Wu, X. Peng, B. Cao, X. Zhang, B. Cao, and G. Cheng. 2015. Editorial: Organic carbon pools in permafrost regions on the Qinghai–Xizang (Tibetan) Plateau. Cryosphere **9**: 479–486. doi:10.5194/tc-9-479-2015

Mu, C. C., and others. 2017. Thaw depth determines dissolved organic carbon concentration and biodegradability on the northern Qinghai–Tibetan Plateau. Geophys. Res. Lett. **44**: 9389–9399. doi:10.1002/2017gl075067

Murphy, K. R., C. A. Stedmon, D. Graeber, and R. Bro. 2013. Fluorescence spectroscopy and multi-way techniques. PARAFAC. Anal. Methods **5**: 6557–6566. doi:10.1039/c3ay41160e

Ohno, T. 2002. Fluorescence inner-filtering correction for determining the humification index of dissolved organic matter. Environ. Sci. Technol. **36**: 742–746. doi:10.1021/es0155276

Qu, B., and others. 2017. Aged dissolved organic carbon exported from rivers of the Tibetan Plateau. PloS One **12**: e0178166. doi:10.1371/journal.pone.0178166

Savory, J. J., N. K. Kaiser, A. M. McKenna, F. Xian, G. T. Blakney, R. P. Rodgers, C. L. Hendrickson, and A. G. Marshall. 2011. Parts-per-billion Fourier transform ion cyclotron resonance mass measurement accuracy with a "walking" calibration equation. Anal. Chem. **83**: 1732–1736. doi:10.1021/ac102943z

Schuur, E. A., and others. 2015. Climate change and the permafrost carbon feedback. Nature **520**: 171–179. doi:10.1038/nature14338

Shen, Y., and R. Benner. 2020. Molecular properties are a primary control on the microbial utilization of dissolved organic matter in the ocean. Limnol. Oceanogr. **65**: 1061–1071. doi:10.1002/lno.11369

Shirokova, L. S., A. V. Chupakov, S. A. Zabelina, N. V. Neverova, D. Payandi-Rolland, C. Causserand, J. Karlsson, and O. S. Pokrovsky. 2019. Humic surface waters of frozen peat bogs (permafrost zone) are highly resistant to bio- and photodegradation. Biogeosciences **16**: 2511–2526. doi:10.5194/bg-16-2511-2019

Smith, D. F., D. C. Podgorski, R. P. Rodgers, G. T. Blakney, and C. L. Hendrickson. 2018. 21 Tesla FT-ICR mass spectrometer for ultrahigh-resolution analysis of complex organic mixtures. Anal. Chem. **90**: 2041–2047. doi:10.1021/acs.analchem.7b04159

Spencer, R. G. M., W. Guo, P. A. Raymond, T. Dittmar, E. Hood, J. Fellman, and A. Stubbins. 2014. Source and biolability of ancient dissolved organic matter in glacier and lake ecosystems on the Tibetan Plateau. Geochim. Cosmochim. Acta **142**: 64–74. doi:10.1016/j.gca.2014.08.006

Spencer, R. G. M., P. J. Mann, T. Dittmar, T. I. Eglinton, C. McIntyre, R. M. Holmes, N. Zimov, and A. Stubbins. 2015. Detecting the signature of permafrost thaw in Arctic rivers. Geophys. Res. Lett. **42**: 2830–2835. doi:10.1002/2015gl063498

Stedmon, C. A., S. Markager, and R. Bro. 2003. Tracing dissolved organic matter in aquatic environments using a new approach to fluorescence spectroscopy. Mar. Chem. **82**: 239–254. doi:10.1016/s0304-4203(03)00072-0

Tarnocai, C., J. G. Canadell, E. A. G. Schuur, P. Kuhry, G. Mazhitova, and S. Zimov. 2009. Soil organic carbon pools in the northern circumpolar permafrost region. Glob. Biogeochem. Cycles **23**. doi:10.1029/2008gb003327

Vonk, J. E., and others. 2013. High biolability of ancient permafrost carbon upon thaw. Geophys. Res. Lett. **40**: 2689–2693. doi:10.1002/grl.50348

Wang, Y. H., and others. 2018*a*. Selective leaching of dissolved organic matter from alpine permafrost soils on the Qinghai–Tibetan Plateau. J. Geophys. Res.: Biogeosci. **123**: 1005–1016. doi:10.1002/2017jg004343

Wang, Y. H., and others. 2018*b*. Spatiotemporal transformation of dissolved organic matter along an alpine stream flow path on the Qinghai–Tibet Plateau: Importance of source and permafrost degradation. Biogeosciences **15**: 6637–6648. doi:10.5194/bg-15-6637-2018

Wang, T. H., D. Yang, Y. Yang, S. Piao, X. Li, G. Cheng, and B. Fu. 2020*a*. Permafrost thawing puts the frozen carbon at risk over the Tibetan Plateau. Sci. Adv. **6**: eaaz3513. doi:10.1126/sciadv.aaz3513

Wang, Y. H., Y. P. Xu, D. D. Wei, L. L. Shi, Z. H. Jia, and Y. H. Yang. 2020*b*. Different chemical composition and storage mechanism of soil organic matter between active and permafrost layers on the Qinghai–Tibetan Plateau. J. Soil. Sediments **20**: 653–664. doi:10.1007/s11368-019-02462-9

Wang, G. Q., and others. 2022. Divergent trajectory of soil autotrophic and heterotrophic respiration upon permafrost thaw. Environ. Sci. Technol. **56**: 10483–10493. doi:10.1021/acs.est.1c07575

Ward, C. P., and R. M. Cory. 2016. Complete and fartial fhoto-oxidation of dissolved organic matter draining permafrost soils. Environ. Sci. Technol. **50**: 3545–3553. doi:10.1021/acs.est.5b05354

Ward, C. P., S. G. Nalven, B. C. Crump, G. W. Kling, and R. M. Cory. 2017. Photochemical alteration of organic carbon draining permafrost soils shifts microbial metabolic pathways and stimulates respiration. Nat. Commun. **8**: 772. doi:10.1038/s41467-017-00759-2

Weishaar, J. L., G. R. Aiken, B. A. Bergamaschi, M. S. Fram, R. Fujii, and K. Mopper. 2003. Evaluation of specific

ultraviolet absorbance as an indicator of the chemical composition and reactivity of dissolved organic carbon. Environ. Sci. Technol. **37**: 4702–4708. doi:10.1021/es030360x

Wickland, K. P., G. R. Aiken, K. Butler, M. M. Dornblaser, R. G. M. Spencer, and R. G. Striegl. 2012. Biodegradability of dissolved organic carbon in the Yukon River and its tributaries: Seasonality and importance of inorganic nitrogen. Glob. Biogeochem. Cycles **26**. doi:10.1029/2012gb004342

Wilson, H. F., and M. A. Xenopoulos. 2009. Effects of agricultural land use on the composition of fluvial dissolved organic matter. Nat. Geosci. **2**: 37–41. doi:10.1038/Ngeo391

Xian, F., C. L. Hendrickson, G. T. Blakney, S. C. Beu, and A. G. Marshall. 2010. Automated broadband phase correction of Fourier transform ion cyclotron resonance mass spectra. Anal. Chem. **82**: 8807–8812. doi:10.1021/ac101091w

Yang, G., and others. 2018. Changes in methane flux along a permafrost thaw sequence on the Tibetan Plateau. Environ. Sci. Technol. **52**: 1244–1252. doi:10.1021/acs.est.7b04979

Yang, X. F., W. M. Qin, L. C. Wang, M. Zhang, and Z. G. Niu. 2021. Long-term variations of surface solar radiation in China from routine meteorological observations. Atmos. Res. **260**: 105715. doi:10.1016/j.atmosres.2021.105715

Yu, P., Z. Guo, T. Wang, J. Wang, Y. Guo, and L. Zhang. 2023. Insights into the mechanisms of natural organic matter on the photodegradation of indomethacin under natural sunlight and simulated light irradiation. Water Res. **244**: 120539. doi:10.1016/j.watres.2023.120539

Acknowledgments

This work was financially supported by the Science and Technology Innovation Plan Of Shanghai Science and Technology Commission (Grant #23230760300) and the National Basic Research Program of China (Grant #2014CB954001). The Ion Cyclotron Resonance user facility at the National High Magnetic Field Laboratory is supported by the National Science Foundation Division of Materials Research and Division of Chemistry through DMR-2128556 and the State of Florida. We are grateful to Futing Liu and Dandan Wei for their assistance in the fieldwork.

Submitted 12 October 2023
Revised 07 March 2024
Accepted 11 March 2024